

#### **OPEN ACCESS**

EDITED BY

Chrysanthos Maraveas, Agricultural University of Athens, Greece

#### REVIEWED BY

Marianna Kotzampasaki, Agricultural University of Athens, Greece Konstantina Filippou, Agricultural University of Athens, Greece Kai Xin, Michigan Technological University,

\*CORRESPONDENCE

**United States** 

Zhe Li,

□ nmgjttlz@163.com

RECEIVED 14 August 2025 REVISED 29 October 2025 ACCEPTED 03 November 2025 PUBLISHED 20 November 2025

#### CITATION

Li Z, Wei X, Hou G, Xing Y and Wang D (2025) Research on the coupling effect of film thickness and UV aging cycle on the rheological properties and microstructure evolution law of asphalt. Front. Mater. 12:1685828. doi: 10.3389/fmats.2025.1685828

#### COPYRIGHT

© 2025 Li, Wei, Hou, Xing and Wang. This is an open-access article distributed under the terms of the Creative Commons Attribution License (CC BY). The use, distribution or reproduction in other forums is permitted, provided the original author(s) and the copyright owner(s) are credited and that the original publication in this journal is cited, in accordance with accepted academic practice. No use, distribution or reproduction is permitted which does not comply with these terms.

# Research on the coupling effect of film thickness and UV aging cycle on the rheological properties and microstructure evolution law of asphalt

Zhe Li<sup>1,2</sup>\*, Xuefeng Wei<sup>3</sup>, Gui Hou<sup>2</sup>, Yadong Xing<sup>3</sup> and Dengyong Wang<sup>3</sup>

<sup>1</sup>Changsha University of Science and Technology School of Transportation, Changsha, China, <sup>2</sup>Inner Mongolia Autonomous Region Transportation Science Development Research Institute, Hohhot, China, <sup>3</sup>Ulanqab Transportation Resources Development Group Co., Ltd, Ulanqab, China

In high-altitude regions, intense ultraviolet (UV) radiation significantly accelerates the aging of road asphalt. However, there is currently a lack of corresponding UV aging standard tests. This study addresses this issue by designing a programmable, adjustable-intensity indoor UV aging test to more accurately simulate the strong UV environment found at high altitudes. This study examines the effects of varying UV aging cycles and asphalt film thicknesses on the rheological properties and micro-aging mechanisms of 90# asphalt. Employing tests such as the dynamic shear rheometer, multi-stress creep recovery, and linear amplitude sweep, the study quantifies the impact of UV aging on asphalt's high-temperature stability, deformation recovery capacity, and fatigue life. In conjunction with analyses via Fourier Transform Infrared Spectroscopy (FTIR), Scanning Electron Microscopy (SEM), and Atomic Force Microscopy (AFM), this research elucidates the evolution of chemical functional groups under UV irradiation, characterizes micro-crack propagation through five distinct stages, and reveals the underlying mechanisms governing changes in 'bee structures.' The findings indicate that UV aging significantly increases the asphalt's high-temperature rutting factor by up to 303% for a 1 mm film after 9 cycles, and decreases its unrecoverable creep compliance by as much as 35.9%. This hardening, however, ultimately impairs its fatigue performance, with fatigue life reduced by up to 25.0%. The thickness of the asphalt film is identified as a crucial factor influencing the depth of aging, with thinner layers undergoing more severe aging. On a microstructural level, FTIR analysis confirmed an increase in carbonyl ( $I_{C=O}$ ) and sulfoxide ( $I_{S=O}$ ) functional group indices and a decrease in the aromatic compounds (I<sub>Ar</sub>) index. Concurrently, surface damage progressed from micro-wrinkling to macro-cracking, and the average area of 'bee structures' in the most severely aged sample (1 mm-9C) increased by 248% compared to the unaged asphalt. This research provides key theoretical insights and quantitative data support for material selection, durability design, and lifespan prediction of asphalt pavements in areas with intense UV

radiation, offering a conceptual framework for developing standardized asphalt aging tests.

KEYWORDS

ultraviolet aging, asphalt aging, asphalt, rheological properties, microscopic mechanism

# 1 Introduction

Asphalt is the primary binding material of asphalt pavements, and its properties significantly influence the lifespan and quality of the roads. During their service life, asphalt inevitably undergoes an aging process that leads to performance degradation, with ultraviolet (UV) aging being a key factor in the premature deterioration of asphalt pavements (Guo et al., 2023; He et al., 2025b). The degradation of mechanical properties of various polymer materials by ultraviolet radiation has been generally regarded as the key cause of their degradation (Maraveas et al., 2023; Maraveas et al., 2024). Prolonged exposure of asphalt materials to high-intensity UV radiation accelerates photochemical reactions, resulting in issues such as hardening, brittleness, and surface cracking, which severely shorten the road's lifespan and increase maintenance costs (Polo-Mendoza et al., 2022). Therefore, an in-depth study of the UV aging behavior of asphalt in such environments and its mechanisms is crucial for enhancing road durability, holding significant theoretical and engineering value.

Currently, researchers both domestically and internationally have conducted a series of studies on the UV aging behavior of asphalt. It is widely recognized that UV exposure promotes the formation of carbonyl and sulfoxide groups in asphalt (Xiao and Fan, 2022; Wang et al., 2024a), altering its chemical composition and microstructure, which in turn affects its macroscopic rheological properties (Li et al., 2025). Clara Celauro (Celauro et al., 2022) demonstrated through FTIR experiments that, after UV aging, SBS-modified asphalt exhibits an increased ratio of carbonyl and hydroxyl groups, indicating the formation of a substantial number of oxygen-containing groups, which suggests degradation under UV irradiation. Notably, higher-grade asphalts were found to be less susceptible to UV degradation. Zhengang Feng (Feng et al., 2016) separated the four components of asphalt and conducted UV aging tests on each, with FTIR results showing that all four components undergo complex reactions such as oxidation and aromaticity. It was observed that saturated hydrocarbons, particularly olefins, are more prone to destruction and oxidation by UV radiation. Siddiqui M (Siddiqui and Ali, 1999) proposed that the mechanism of photooxidation can explain the aging process of asphalt under UV light. When asphalt is exposed to UV radiation, C-C, C-H, and C=C bonds within the material break, forming free radicals. This manifests macroscopically as an increase in hardness and brittleness, resulting in higher overall resistance to stress, an elevated storage modulus, a reduced loss modulus, and an increased complex shear modulus (Airey et al., 2016; Godenzoni et al., 2017; Capayova et al., 2022). Concurrently, asphalt transitions from a viscoelastic state to an elastic state, accompanied by a decrease in phase angle (Zhang et al., 2017; Carmona et al., 2023). Yuanyaun Li (Li et al., 2019a) evaluated the effects of UV light at different wavelengths on asphalt using phase angle and complex modulus, finding that the complex modulus increased with loading frequency, while the phase angle decreased. Xiaolong Sun (Sun et al., 2022) compared 70# asphalt before and after UV aging, with multi-stress creep recovery (MSCR)tests indicating that the elastic recovery performance of 70# asphalt declines significantly and its resistance to deformation decreases with prolonged UV aging.

However, existing research often relies on corresponding aging duration and UV intensity to achieve realistic simulations of UV aging effects (Cong et al., 2012; Feng et al., 2016; Zadshir et al., 2018; Chen et al., 2020). The results of Mouillet V (Mouillet et al., 2014) indicate that there is a logarithmic relationship between the extent of UV aging of asphalt and UV exposure time. Therefore, employing such equivalent substitutions may not effectively mimic real pavement conditions. To address this limitation, this study simulates UV aging using the actual local UV intensity over several cycles. The penetration depth of UV radiation into asphalt is severely limited, typically to only tens to hundreds of micrometers. This physical limitation implies that for asphalt films thicker than this penetration depth, only the surface layer is directly affected by UV light. Consequently, the overall degree of aging of a sample becomes a function of the volumetric ratio of the "aged surface layer" to the "unaged bulk material," which makes film thickness a potentially dominant variable (He et al., 2025a). The findings reveal that the penetration depth of UV light is limited, and the thickness of the asphalt film is undoubtedly a critical factor affecting both the rate and extent of aging (Zeng et al., 2018). Durrieu Françoise (Durrieu et al., 2007) conducted UV aging experiments using 10 µm asphalt films, and the results showed that after only a few hours, the aging extent reached the level observed in pressure aging vessel (PAV) aging. Jinxuan Hu (Hu et al., 2017) and colleagues investigated the aging effects of asphalt samples with thicknesses of 50 μm, 100 μm, 200 μm, and 500 μm under identical UV exposure conditions. The extent of UV aging is closely related to the thickness of the asphalt samples, with thicker samples exhibiting a lower glass transition temperature post-aging. However, systematic and multiscale comparative studies on the aging behavior of asphalt under high UV conditions at different film thicknesses still require further investigation. Additionally, the intrinsic mechanisms linking the evolution of asphalt's macroscopic properties with changes in its microchemical structure and surface morphology damage under these specific aging conditions also need to be elucidated.

Therefore, this study focuses on 90# asphalt and employs a programmable UV aging testing method designed based on actual solar shortwave radiation data from the Naqu region. It systematically investigates the effects of different UV aging cycles and asphalt film thickness on both the rheological properties and micro-aging mechanisms. Temperature scanning, multi-stress creep recovery (MSCR), and linear amplitude sweep (LAS) tests are conducted using a dynamic shear rheometer (DSR). Additionally, microscopic characterization techniques, including

TABLE 1 Technical parameters and test results of 90# asphalt.

Т	echnical item	Unit	Standard requirements	Test result	Testing method
Penetration (25 ℃)		0.1 mm	80~100	87	ASTM D5
Penetration index		_	≥-2.5 -1.1		ASTM D5
Softening point		℃	≥44	45.5	ASTM D36
Ductility (15 ℃)		cm	≥100	110	ASTM D113
Viscosity (60 ℃)		Pa∙s	≥140	142	ASTM D4402
Flash point		℃	≥245	256	ASTM D92
Solubility		%	≥99.5	≥99.5 99.9	
Density		g/cm <sup>3</sup>	_	1.025	ASTM D70
RTFOT	Mass variation	%	≤±0.8	-0.06	
	Penetration ratio (25 ℃)	%	≥57	59	ASTM D2872
	Ductility (10 ℃)	cm	≥8	8.9	

Fourier transform infrared spectroscopy (FTIR), scanning electron microscopy (SEM), and atomic force microscopy (AFM), are utilized to reveal the aging patterns of asphalt simulated under high-altitude, strong UV conditions. This study aims to quantify the film thickness effect and elucidate the multi-scale damage evolution mechanisms, providing a more precise theoretical basis and data support for the durability design and performance prediction of asphalt pavement materials in high-altitude regions.

#### 2 Materials and tests

# 2.1 Asphalt

In high-altitude regions characterized by intense ultraviolet exposure, 90# asphalt and SBS-modified asphalt are commonly employed as binding materials. These materials possess a high content of saturated and aromatic compounds, which can dissipate UV energy through the conjugated structure of their molecular chains, thereby offering both UV brittleness resistance and low-temperature crack resistance (Zhou et al., 2024; Ren et al., 2025). However, to explore the effects of UV light on asphalt, it is important to note that SBS-modified asphalt requires the addition of 3%–5% polymer modifiers and other stabilizers during production, which complicates the consistency of the experimental samples' performance. To eliminate extraneous interference, this study selects 90# asphalt produced by Panjin Dali Petrochemical Company, with its technical specifications listed in Table 1.

#### 2.2 Ultraviolet aging test design

Based on ultraviolet monitoring data from the Naqu Meteorological Bureau covering the period from January 1, 1980, to

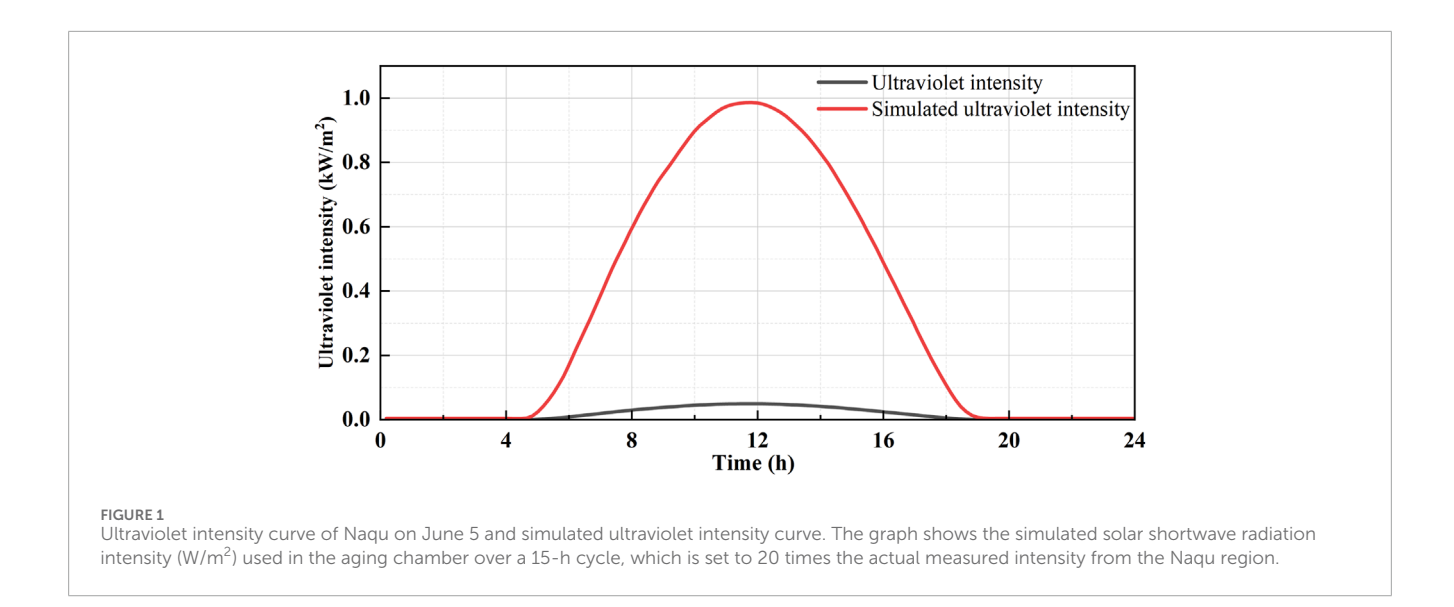
TABLE 2 Correspondence table between outdoor ultraviolet (UV) exposure time and simulated UV exposure time.

Duration of outdoor ultraviolet exposure(d)	Cycle
20	1
60	3
120	6
180	9

December 31, 2010, this study selects the solar shortwave radiation data from June 5, a representative day in summer, as a benchmark. A programmable UV aging chamber that automatically adjusts UV intensity is used to simulate solar shortwave radiation. The UV intensity is automatically adjusted according to the actual shortwave radiation curve, with each experimental cycle lasting 15 h. To achieve accelerated aging of the asphalt materials, the UV intensity is set to 20 times that of the actual shortwave radiation. The correspondence between the indoor simulation time and the outdoor UV exposure time is detailed in Table 2. It should be noted that this programmable loop, although based on actual regional data, represents a standardized and simplified simulation. It deliberately maintains a constant temperature to isolate the effects of UV radiation and does not consider other complex environmental variables such as humidity, precipitation, cloud cover, or daily temperature fluctuations, which likewise affect the aging process on site.

The experiments show that asphalt molecules have different sensitivity to different wavelengths of ultraviolet rays, and ultraviolet rays with wavelengths of 360–370 nm have the greatest influence on the macroscopic rheological properties

10.3389/fmats.2025.1685828 Li et al



and microscopic characteristics of asphalt (Li et al., 2019b). This study utilizes a 360 nm LED UV lamp as the light source for the UV aging test. During the UV exposure process, the ambient temperature is maintained at the local average of 30 °C to ensure that the observed aging effects are primarily attributed to UV radiation. The measurement of UV irradiance is conducted using a UV intensity meter, with the testing probe positioned 15 cm vertically from the sample surface to measure the light intensity. The resulting intensity-time curve is illustrated in Figure 1.

The thickness of the asphalt film is a crucial factor affecting the effects of UV aging. Based on a literature review, asphalt film thicknesses of 1 mm, 1.5 mm, and 2 mm were selected for this study. UV aging asphalt samples were prepared based on these thicknesses by controlling the mass of the asphalt. As shown in Figure 2A, pitch preheated at 140 °C for 1 h was poured into an aging pan according to the specified mass and then placed in an oven at 140 °C. The asphalt was heated for 15 min to ensure it was evenly spread. For simplicity, the asphalt with a film thickness of 1 mm aged under the conditions of 3 UV cycles will be referred to as 1 mm-3C, and other samples will be designated similarly based on their respective conditions. Three parallel specimens were prepared for each type of asphalt mixture; each test was performed three times, and the average value was taken as the test result.

As shown in Figure 2B, after UV aging, the aged asphalt is heated at 140 °C for 15 min, stirred for 60 s, and then heated for an additional 15 min before sampling for subsequent tests.

## 2.3 Rheological test

To investigate the effects of UV aging on the rheological properties of 90# asphalt, this study employs the Anton Paar Model 302 DSR, conducting experiments by AASHTO standard testing methods.

Temperature scanning tests are carried out within the range of 46 °C-88 °C, with a temperature gradient of 6 °C. The strain value

 $(\gamma)$  is set at 12%, and the angular frequency  $(\omega)$  is set to 10 rad/s. The multi-stress creep recovery tests are performed at 58 °C, applying loads of 0.1 kPa and 3.2 kPa. The measured parameters include creep recovery rate, percentage difference in creep recovery, unrecoverable creep compliance, and its percentage difference. Linear amplitude sweep tests are conducted at 25 °C to evaluate the linear viscoelastic properties of the materials.

#### 2.4 FTIR test

This study employed the Thermo Scientific iS50 FTIR system for the experiments. FTIR analysis was conducted to investigate the changes in the functional groups of asphalt resulting from UV aging. Infrared spectra were recorded over a wavenumber range of 4,000 cm<sup>-1</sup> to 400 cm<sup>-1</sup>, with a total of 32 scans performed at a spectral resolution of 4 cm<sup>-1</sup>.

Since infrared spectral results can be significantly influenced by concentration, calculating the absolute values of peak areas for comparison is not particularly meaningful. Therefore, a relative content analysis was performed for each asphalt sample. The peak area was quantified to compute the indices for branched aliphatic functional groups (I<sub>B</sub>), aromatic functional groups (I<sub>Ar</sub>), carbonyl functional groups  $(I_{C=0})$ , and sulfoxide functional groups  $(I_{S=0})$ using Formulas 1-6.

$$I_B = \frac{A_{1377}}{A_{1462} + A_{1377}} \tag{1}$$

$$I_{Ar} = \frac{A_{1600}}{\sum A} \tag{2}$$

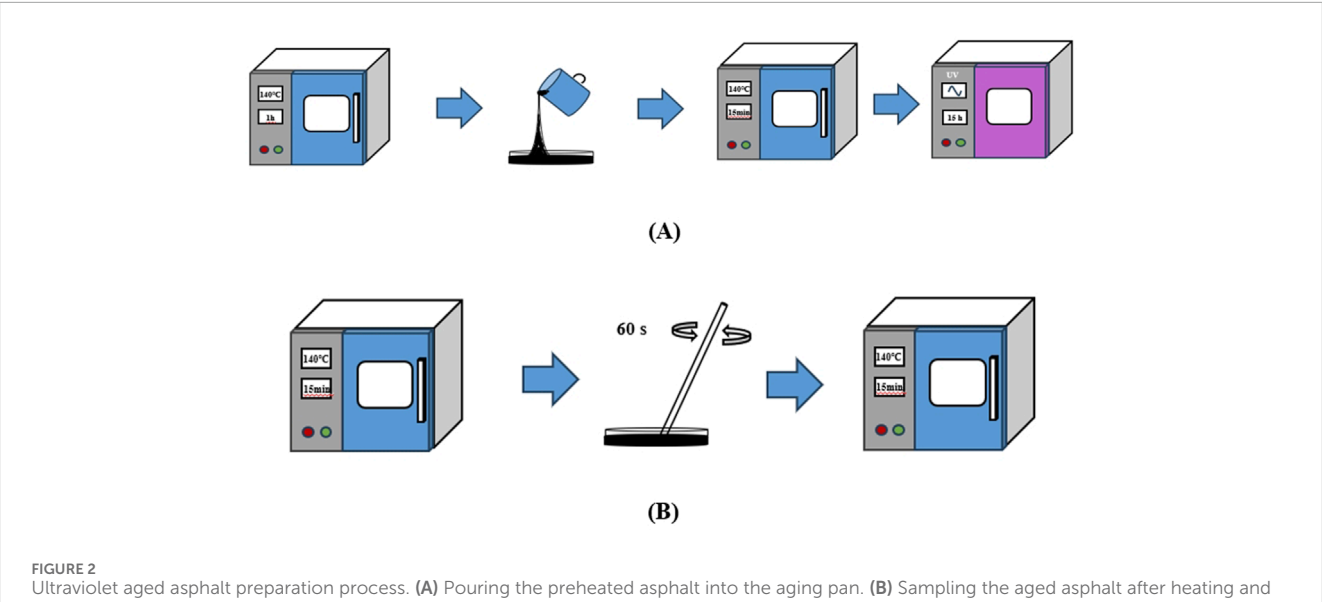
$$I_{C=O} = \frac{A_{1700}}{\sum A} \tag{3}$$

$$I_{C=O} = \frac{A_{1700}}{\sum A}$$

$$I_{S=O} = \frac{A_{1030}}{\sum A}$$
(4)

$$\sum A = A_{(2925,2855)} + A_{1700} + A_{1600} + A_{1540} + A_{1460} + A_{1370} + A_{1030} + A_{966} + A_{875} + A_{815} + A_{745}$$
(5)

10.3389/fmats.2025.1685828 Li et al



stirring for subsequent tests.

$$W = \frac{I_{aged} - I_{unaged}}{I_{unaged}} * 100\%$$
 (6)

I<sub>B</sub> represents the branched aliphatic functional group index, IAr denotes the aromatic functional group index, IC=O indicates the carbonyl functional group index, and I<sub>S=O</sub> corresponds to the sulfoxide functional group index. Axxxx refers to the corresponding peak area, while W represents the rate of change of each functional group in the asphalt with aging.

The terms  $I_B$ ,  $I_{Ar}$ ,  $I_{C=O}$ , and  $I_{S=O}$  denote the functional group indices for branched aliphatic, aromatic, carbonyl, and sulfoxide groups, respectively. Additionally, Axxxx refers to a corresponding peak area, and W represents the rate of change for each functional group in asphalt during aging.

#### 2.5 AFM test

AFM was employed to analyze changes in the surface morphology of asphalt due to UV aging. Using the tapping mode, a scanning frequency of 1 Hz, a scanning area of 20  $\mu$ m  $\times$  20  $\mu$ m, and a resolution of 512 ppi × 512 ppi, each sample was scanned at three different points.

#### 2.6 SEM test

To observe the impact of UV aging on the micro-morphology of 90# asphalt, this study utilized SEM to characterize the sample surfaces. The analysis compared the micro-morphologies before and after aging, ensuring that the surfaces were not disturbed by external forces, to assess the effects of UV exposure on the structure of the surface layer of the asphalt. SEM testing was conducted at an accelerating voltage of 10 kV, utilizing magnifications of 100x and 200x for imaging observations.

# 3 Rheological test results

# 3.1 Results of the temperature-frequency scanning test

The SHRP program employs the rutting factor G\*/sinδ from DSR testing as an evaluation criterion for the high-temperature performance of asphalt. Zhang (Zhang et al., 2018) research shows that A smaller amount of energy dissipated due to the viscous flow deformation of the material corresponds to a larger G\*/sinδ value, indicating better rutting resistance for the asphalt material; conversely, a larger amount of dissipated energy reflects poorer rutting resistance. The temperature scanning test results for UV-aged asphalt are shown in Figure 3.

The extent of this improvement is highly dependent on both the film thickness and the number of aging cycles, as quantified in Table 3. The most critical factor influencing the degree of aging is the film thickness; under the same aging duration, the rutting factor increases as the film thickness decreases. For any given film thickness, the rutting factor also increases progressively with more aging cycles.

These coupled effects are most pronounced in the 1 mm film samples. After 9 cycles, the rutting factor for the 1 mm film increased by over 300%, while the 2 mm film showed a more modest increase of 82% under the same conditions. This demonstrates that thinner films undergo more severe oxidative hardening due to the greater relative penetration of UV radiation. This hardening results in a stiffer, more elastic-dominant material with superior resistance to permanent deformation at high temperatures. This is consistent with the results of Chen Zihao's layered analysis of asphalt membranes with a thickness of several millimeters or microns in the ultraviolet aging experiment of asphalt (Chen et al., 2020).

Furthermore, the value of G\*/sin δ decreases with increasing temperature, and the slope of this decrease characterizes the sensitivity of the material's rheological properties to temperature

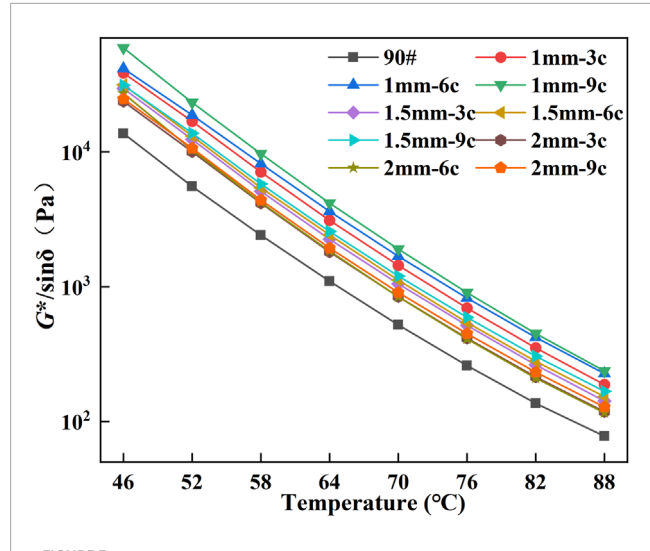


FIGURE 3
Results of the temperature scanning test for UV-aged aspha. The graphs show the rutting factor as a function of temperature for asphalt samples with film thicknesses of 1 mm, 1.5 mm, and 2 mm, each subjected to 3, 6, and 9 UV aging cycles.

variations. Moreover, as shown in Figure 3, the slopes of the  $G^*/\sin \delta$ –temperature curves remain relatively parallel under different aging conditions. This indicates that although UV aging significantly hardens the asphalt, it does not markedly alter its temperature sensitivity within the tested range of 46 °C–88 °C.

#### 3.2 Analysis results of the aging index

The aging index of asphalt can be calculated by measuring the ratio of the rutting factors before and after aging. This ratio serves as an indicator, reflecting the differences in the high-temperature rutting performance of the asphalt material before and after aging, and it can also provide an estimate of the extent of asphalt aging. The formula for calculating the Aging Index (AI) is provided in Equation 7.

$$AI = \frac{G * / \sin \delta_{\text{Aged}}}{G * / \sin \delta_{\text{Unaged}}}$$
 (7)

In this equation,  $(G*/\sin\delta_{Aged})$  represents the rutting coefficient of asphalt after UV aging, while  $(G*/\sin\delta_{Unaged})$  denotes the rutting coefficient of 90# asphalt. AI is defined as the Aging Index.

The results clearly demonstrate that film thickness is the dominant factor controlling the AI. As shown in Figure 4, thinner films consistently exhibit significantly higher AI, indicating a more severe degree of aging. For any given film thickness, the AI also increases with the number of aging cycles, although this effect is less pronounced than that of film thickness.

The dominance of film thickness is particularly evident after 9 aging cycles, where the AI of the 1 mm film was approximately 147% higher than that of the 2 mm film. This confirms that the aging effect is concentrated on the surface due to the limited penetration depth of UV light. In thinner samples, this aged surface layer constitutes

a larger proportion of the total sample volume, resulting in a much higher overall measured degree of aging.

Consequently, as film thickness increases, the influence of additional aging cycles becomes progressively less significant. For the 2 mm thick film, the AI changes only slightly between 3 and 9 aging cycles. This suggests that the surface has reached an advanced state of aging, and further UV exposure has a diminished effect on the bulk properties of the thick sample.

The increment of the Aging Index, denoted as  $\Delta$ AI, is calculated according to Equations 8–10. The recalculated data is then stacked and plotted, as shown in Figure 5.

$$\Delta AI_{3C} = AI_{3cycles} - 1 \tag{8}$$

$$\Delta AI_{6C} = AI_{6cycles} - AI_{3cycles}$$
 (9)

$$\Delta AI_{9C} = AI_{9cycles} - AI_{6cycles}$$
 (10)

Figure 5 illustrates the changes in the contribution rates of different stages of UV aging to the Aging Index of asphalt over the 0 to 9 cycles. The contribution rates for the first three cycles of UV aging are the highest, accounting for over 60% of the total UV aging contribution. The contribution rate for cycles 3 to 6 is the lowest, while the rate for cycles 6 to 9 is slightly higher than that for cycles 3 to 6. When sorted in descending order of contribution rate, the ranking is  $\Delta AI_{0-3C} > \Delta AI_{6-9C} > \Delta AI_{3-6C}$ . This trend reflects the phased characteristics of the UV aging rate of asphalt: rapid in the early stages, slowing in the middle period, and slightly rebounding in the later stages.

Further comparison across Figure 5 reveals that as the film thickness increases, the contribution rate of aging during the 0 to 3 cycles shows an upward trend. The aging contribution rates for asphalt with 1 mm and 1.5 mm film thicknesses remain relatively stable during the 3 to 6 cycles, while the contribution rate for 2 mm film thickness asphalt shows a slight decline during the 0 to 6 cycles. In the 6 to 9 cycle phase, the contribution rates for asphalt with a 1–2 mm film thickness initially decrease before rising again.

In the early stage of UV aging of asphalt, UV can penetrate to the surface layer of asphalt to a certain depth. As a result, the asphalt binder in this area undergoes a rapid oxidation reaction and the molecular chain breaks. At this stage, the aging speed is faster, and the stiffness of asphalt increases obviously. As aging progresses, oxidation products gradually accumulate on the surface layer, which hinders ultraviolet rays from continuing to penetrate inside, and the aging rate slows down accordingly. The oxidation products of the asphalt surface were visually confirmed in SEM analysis Figure 12, which clearly documented the development of surface damage from microscopic wrinkles to a hard, cracked morphology. This phenomenon is consistent with the findings of UV aging gradients (Chen et al., 2020). According to Fick's law of diffusion, the diffusion flux increases with the concentration gradient. During the aging process, the formation of sulfoxide and carbonyl functional groups creates a distribution in the system that resembles a highconcentration solute. These aging products diffuse towards lower concentration areas. As aging progresses into the 3 to 6 cycle phase, the degree of hardening of the surface asphalt increases, thereby reducing the penetration depth of UV radiation and leading to localized accumulation of aging substances. In the 6 to 9 cycle phase,

TABLE 3	Percentage	increase of	G*/sinδ at 58	°C compared	d to unaged 90	)# asphalt.

Film thickness	After 3 cycles	After 6 cycles	After 9 cycles
1 mm	194%	239%	303%
1.5 mm	140%	112%	124%
2 mm	73%	75%	82%

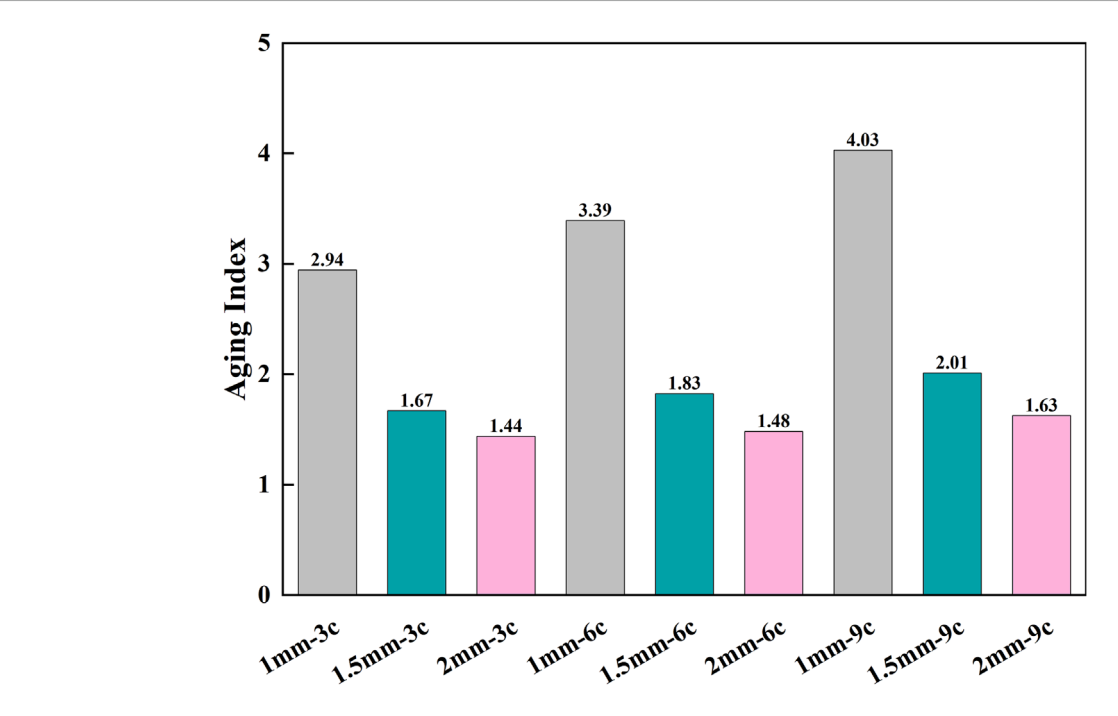


FIGURE 4
Shows the AI of UV-aged asphalt under different aging cycles. The AI, calculated as the ratio of aged to unaged rutting factors, is shown for different film thicknesses and UV aging cycles.

the intensified concentration accumulation accelerates the diffusion process, causing the contribution rate of UV aging to rise again.

#### 3.3 Results of multiple stress creep tests

Asphalt materials exhibit viscoelastic properties, making them susceptible to flow deformation under high temperatures, which can lead to pavement distress. To evaluate their resistance to deformation, this test applies loads at different stress levels to measure the creep behavior of the asphalt material over a specified duration, as well as its recovery capability. The creep recovery rate is an important indicator of the material's ability to resist permanent deformation and reflects its capacity to return to its original shape after being subjected to stress. This characteristic is closely related to the deformation and recovery performance of roads under vehicle loads.

Since the MSCR protocol requires asphalt to undergo short-term aging with the Rolling Thin-Film Oven Test (RTFO) before testing, this study denotes 90#-RTFO as 90# asphalt that has

undergone RTFO treatment. UV-aged asphalt and 90#-RTFO asphalt underwent MSCR testing at temperatures of 58 °C, 64 °C, and 70 °C. The test results indicate that the MSCR tests failed at both 64 °C and 70 °C, while the results from the MSCR test conducted at 58 °C are shown in Figure 6. Figure 6 presents the results of the completed MSCR tests at 58 °C. The creep recovery rate obtained under a stress level of 3.2 kPa was lower than the strain recovery rate obtained at 0.1 kPa, demonstrating that at higher stress levels, the creep recovery rate of asphalt is significantly reduced. With increasing stress levels, the resulting damage and deformation to the asphalt become greater, making recovery more difficult or incomplete in a short time; hence, the creep recovery rate decreases.

All UV-aged asphalts exhibit significantly higher  $R_{0.1}$  and  $R_{3.2}$  values compared to RTFO-aged asphalt. For example, the  $R_{0.1}$  value of 1 mm-9C is 12.14%, and the  $R_{3.2}$  value is 2.10%. This represents an increase of 94% and 250%, respectively, compared to the  $R_{0.1}$  and  $R_{3.2}$  values of RTFO asphalt, which are 6.24% and 0.60%. These results indicate that UV aging significantly enhances the elastic recovery capability of asphalt through photooxidative reactions. Under the same aging cycles, thinner films show higher R values, following the

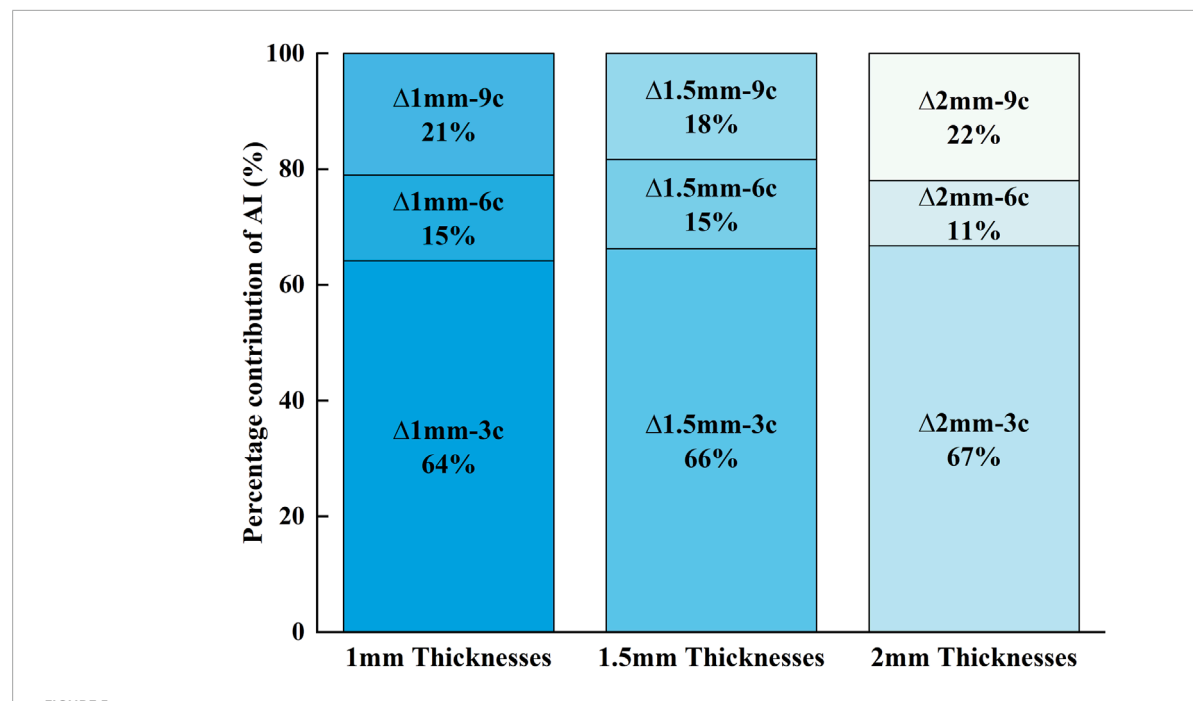
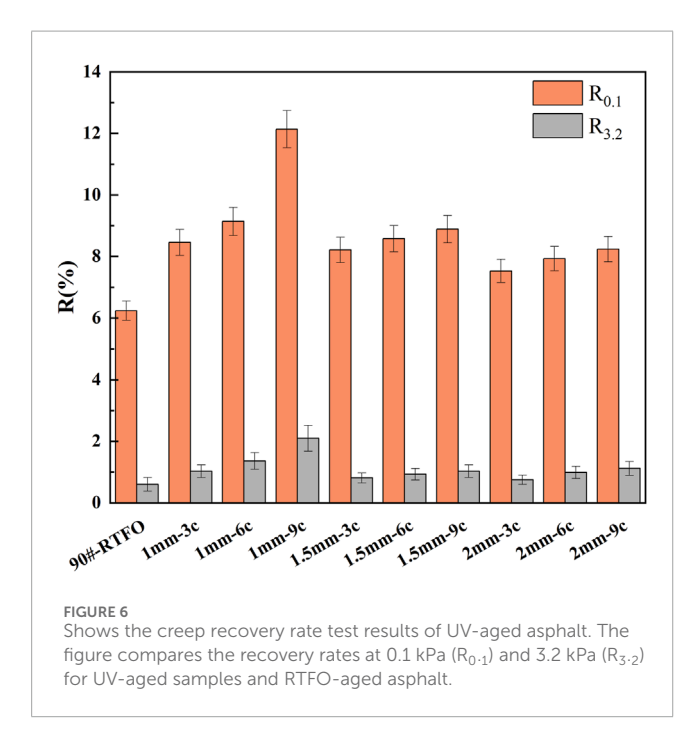


FIGURE 5
Shows the increment of aging index of UV-aged asphalt with different film thicknesses. The stacked bars illustrate the contribution to the total AI from three sequential aging periods: 0-3 cycles ( $\Delta AI_{3C}$ ), 3-6 cycles ( $\Delta AI_{6C}$ ), and 6-9 cycles ( $\Delta AI_{9C}$ ).



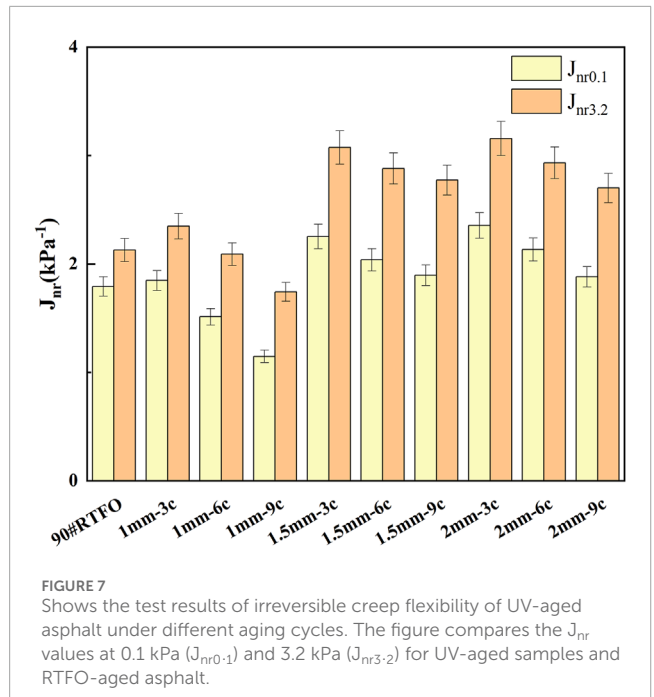
trend of "1 mm > 1.5 mm > 2 mm" Specifically, the  $R_{0.1}$  value for 1 mm asphalt after 9 cycles increased by 43.5% compared to that after 3 cycles, whereas the increase for 2 mm asphalt was only 9.4%. The 1 mm asphalt, due to its greater UV penetration depth, undergoes more uniform oxidation overall, resulting in an increased asphalt content that enhances its elastic recovery capability. In contrast, the 2 mm asphalt mainly experiences aging at the surface, with a

portion of unoxidized components retained in the interior, limiting the increase in its recovery rate. As the film thickness decreases, the enhancing effect of aging cycles on the R value becomes more pronounced.

Additionally, the increase in  $R_{3,2}$  is significantly greater than that in  $R_{0,1}$ , indicating that UV aging has a more pronounced effect on enhancing the elastic recovery capability of asphalt under high stress levels.

When vehicles pass over roadways, the asphalt pavement material experiences deformation due to the vehicle load. This deformation can sometimes be reversible; however, in certain cases, the pavement material undergoes irreversible plastic deformation, known as unrecoverable creep.

As shown in Figure 7, the results of the MSCR tests indicate that as the number of UV aging cycles increases and the film thickness decreases, UV aging significantly reduces the Jnr of asphalt. UV radiation effectively inhibits the permanent deformation of asphalt through photooxidative reactions. Notably, the 1 mm thin layer of asphalt exhibits the lowest Jnr after 9 aging cycles, with J<sub>nr0.1</sub> and J<sub>nr3,2</sub> values of 1.1475 kPa<sup>-1</sup> and 1.7417 kPa<sup>-1</sup>, respectively, which represent reductions of 35.9% and 18.1% compared to RTFO asphalt. As the film thickness increases, the effects of UV aging are significantly diminished; the 2 mm film thickness asphalt reaches a J<sub>nr0.1</sub> of 1.881 kPa<sup>-1</sup> after 9 cycles, which is 64.0% higher than that of the 1 mm sample. Previous research has demonstrated that asphalt film thickness is a critical factor influencing UV aging, with thinner films exhibiting a greater increase in elastic modulus and a higher formation of carbonyl groups compared to thicker ones (Hu et al., 2018). The results of this study are consistent with these findings, as the thicker asphalt films showed a lower oxidation rate under UV irradiation, leading



to less depletion of elastic components and consequently a smaller increase in Jnr.

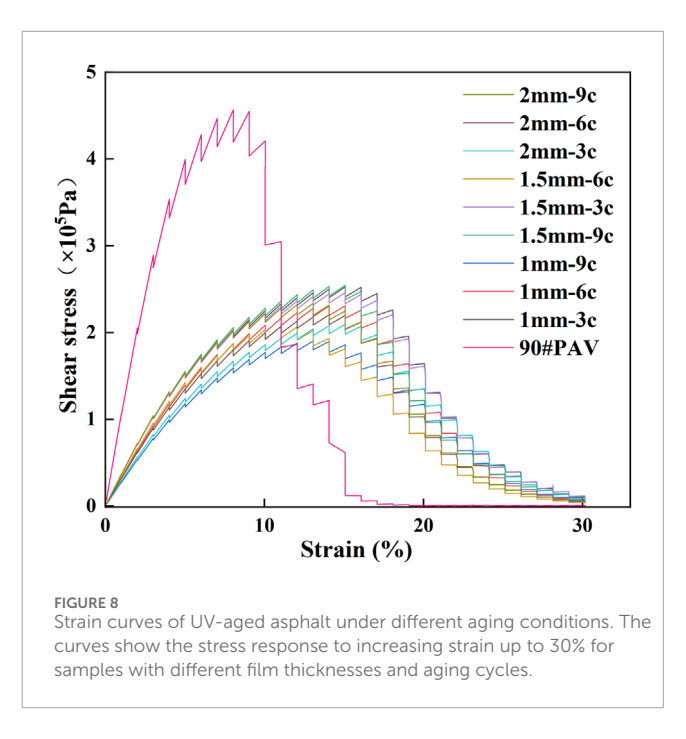
UV light promotes the formation of free radicals, leading to the breakdown of asphalt molecules and an increase in asphaltene content. The increase in asphaltene causes the asphalt to become harder and thicker, thereby enhancing its stress recovery capacity and resistance to deformation, while also reducing its stress relaxation capability.

It is noteworthy that the  $J_{nr0.1}$  and  $J_{nr3.2}$  values for the 1 mm-3C sample are slightly higher than the benchmark values for 90#-RTFO asphalt. The unrecoverable creep compliance for 90#-RTFO asphalt falls between the values of the 1 mm-3C and 1 mm-6C samples. Short-term UV aging may cause the volatilization of light components in asphalt, suggesting that the unrecoverable creep compliance of 90# asphalt can achieve equivalency under specific conditions between thermal oxidative short-term aging and UV aging.

All asphalt samples meet the specifications for  $J_{nr} \le 4.5 \text{ kPa}^{-1}$  at 58 °C, achieving a standard traffic class rating of "S."

#### 3.4 LAS test results

Figure 8 shows the stress-strain curves of asphalt under conditions where 1% strain is incrementally applied every 10 s, resulting in a total strain of 30% over 300 s at 3, 6, and 9 cycles. The curves indicate that both UV-aged asphalt and 90#-PAV asphalt exhibit a distinct inflection point. Beyond this point, as strain increases, the stress gradually decreases. According to the SHRP-A-367 report, asphalt binders exhibit increased brittleness and decreased strength once the stress-strain curve exceeds the ultimate strength. This behavior supports the observation that beyond the inflection point, the stress decreases due to micro-damage and reduced load-carrying capacity of the material (Petersen et al.,



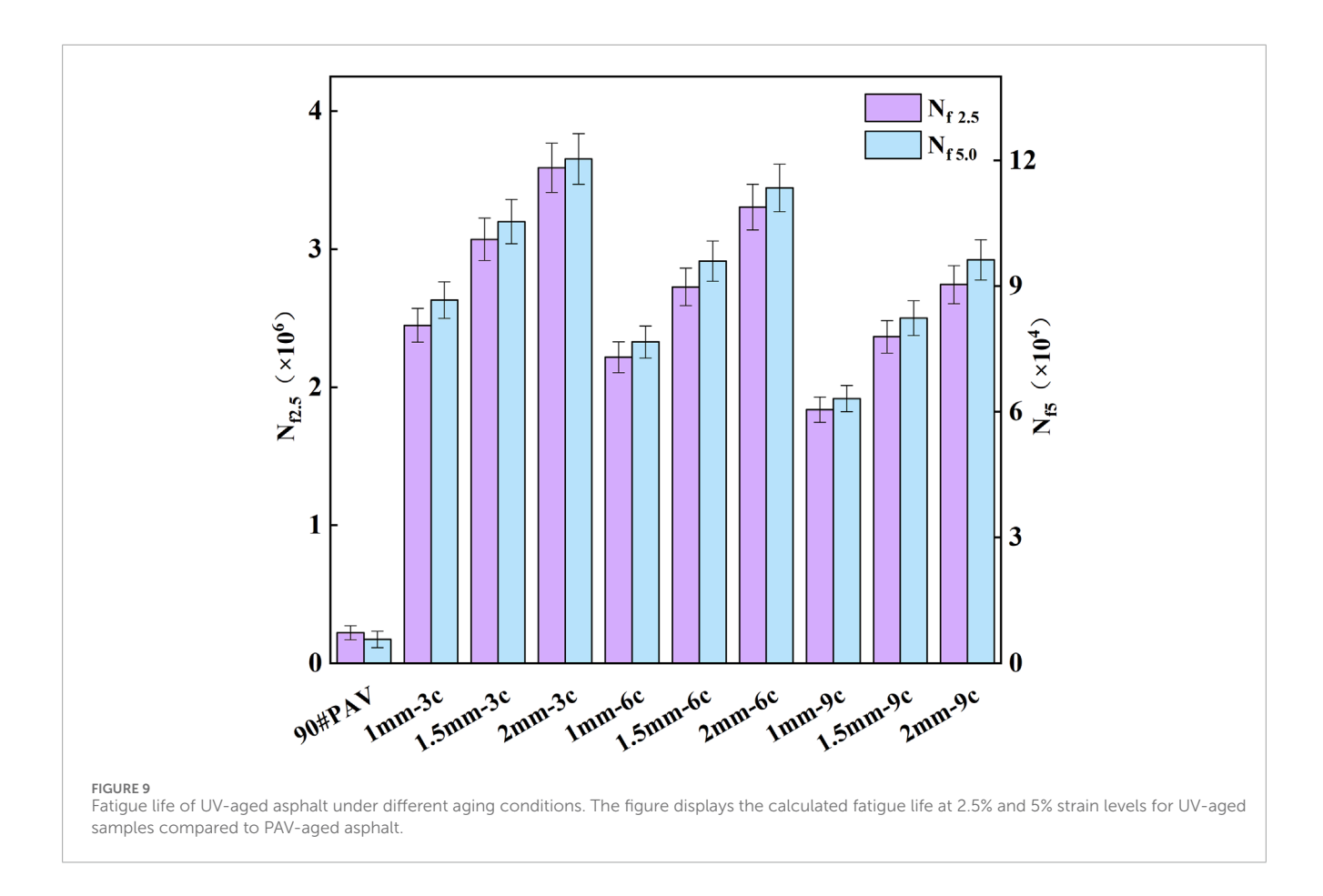
1994). This behavior is attributed to excessive shear stress, which causes damage to the asphalt at the inflection point. Consequently, subsequent increases in strain cannot maintain a high-stress state, leading to a rapid decline in stress levels. Under a strain of 30%, the UV-aged asphalt with thicknesses of 1 mm, 1.5 mm, and 2 mm, along with 90#-PAV asphalt, all fail.

In Figure 9,  $N_{f2.5}$  and  $N_{f5}$  represent the fatigue life counts calculated at strain levels of 2.5% and 5%, respectively. A strain of 5% is applied for low-strength pavements, while 2.5% is used for higher-strength pavements.

The impact of UV aging on the fatigue life of asphalt, shown in Figure 9, reveals a significant nonlinear relationship with film thickness and aging cycles. Compared to PAV-aged asphalt, the data indicate a pronounced aging effect of PAV, which results in fatigue lives that are 9–20 times lower than those of UV-aged asphalt, indicating severe reductions in fatigue life due to prolonged aging.

Under the conditions of 3 UV aging cycles, increasing the asphalt film thickness from 1 mm to 2 mm leads to a 46.6% increase in  $N_{\rm f2.5}$ . After 9 UV aging cycles,  $N_{\rm f2.5}$  values for all film thicknesses decline, with the 2 mm asphalt showing a 23.6% decrease compared to the values after 3 cycles. As the aging progresses from 3 UV cycles to 9 UV cycles, the  $N_{\rm f2.5}$  values for 1 mm and 1.5 mm asphalt decrease by 25.0% and 23.0%, respectively, while the reduction for the 2 mm asphalt is 23.6%. This indicates that UV radiation, through molecular crosslinking and asphaltene enrichment, significantly increases the accumulation of fatigue damage. Wang (Wang et al., 2024b) states that oxidation leads to the loss of light components and the increase of heavy components in asphalt, which in turn leads to low-temperature cracking and reduced fatigue life.

Therefore, under similar conditions, within the range of  $1-2\,\mathrm{mm}$  film thickness, thinner films and longer aging cycles result in lower fatigue lives; the reduction in fatigue life is more pronounced compared to the original asphalt. However, beyond the  $1-2\,\mathrm{mm}$ 



thickness scale, increases in asphalt film thickness have a smaller impact on fatigue life. When the asphalt is too thin, it is prone to excessive aging or even carbonization, making it challenging to accurately assess its fatigue performance.

# 4 Microscopic test results

#### 4.1 Infrared spectroscopy analysis (FTIR)

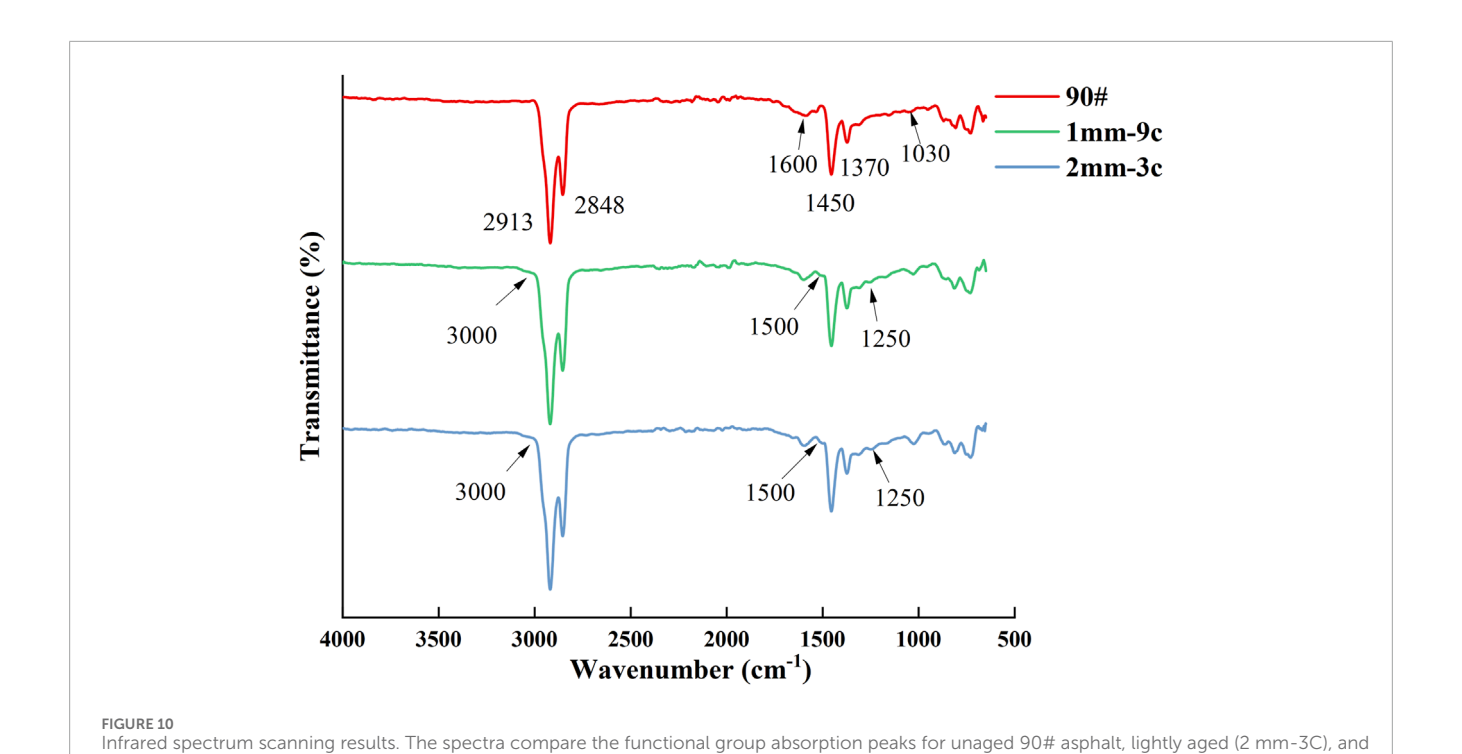
FTIR testing was conducted on asphalt samples with three different film thicknesses and three UV aging cycles, along with 90# asphalt. To analyze the UV aging mechanisms more clearly, the most representative 90# asphalt, the heavily UV-aged 1 mm-9C sample, and the lightly UV-aged 2 mm-3C sample were selected for functional group analysis. The spectra are shown below:

Figure 10 shows that 90# asphalt exhibits distinct absorption bands, with the strongest absorption peaks at 2,931 cm<sup>-1</sup> and 2,848 cm<sup>-1</sup>, primarily attributed to saturated hydrocarbons and their derivatives, CH<sub>2</sub> and CH. The peaks at 1,450 cm<sup>-1</sup> and 1,370 cm<sup>-1</sup> are caused by the stretching vibrations of C-C bonds in alkanes, including C-CH<sub>3</sub> and -CH<sub>2</sub>-. A slight absorption peak at 1,030 cm<sup>-1</sup> indicates the presence of sulfur elements in the asphalt. After UV aging, a distinct stretching vibration signal of sulfoxide groups appears, indicating the formation of S=O double bonds in an oxygen-rich environment.

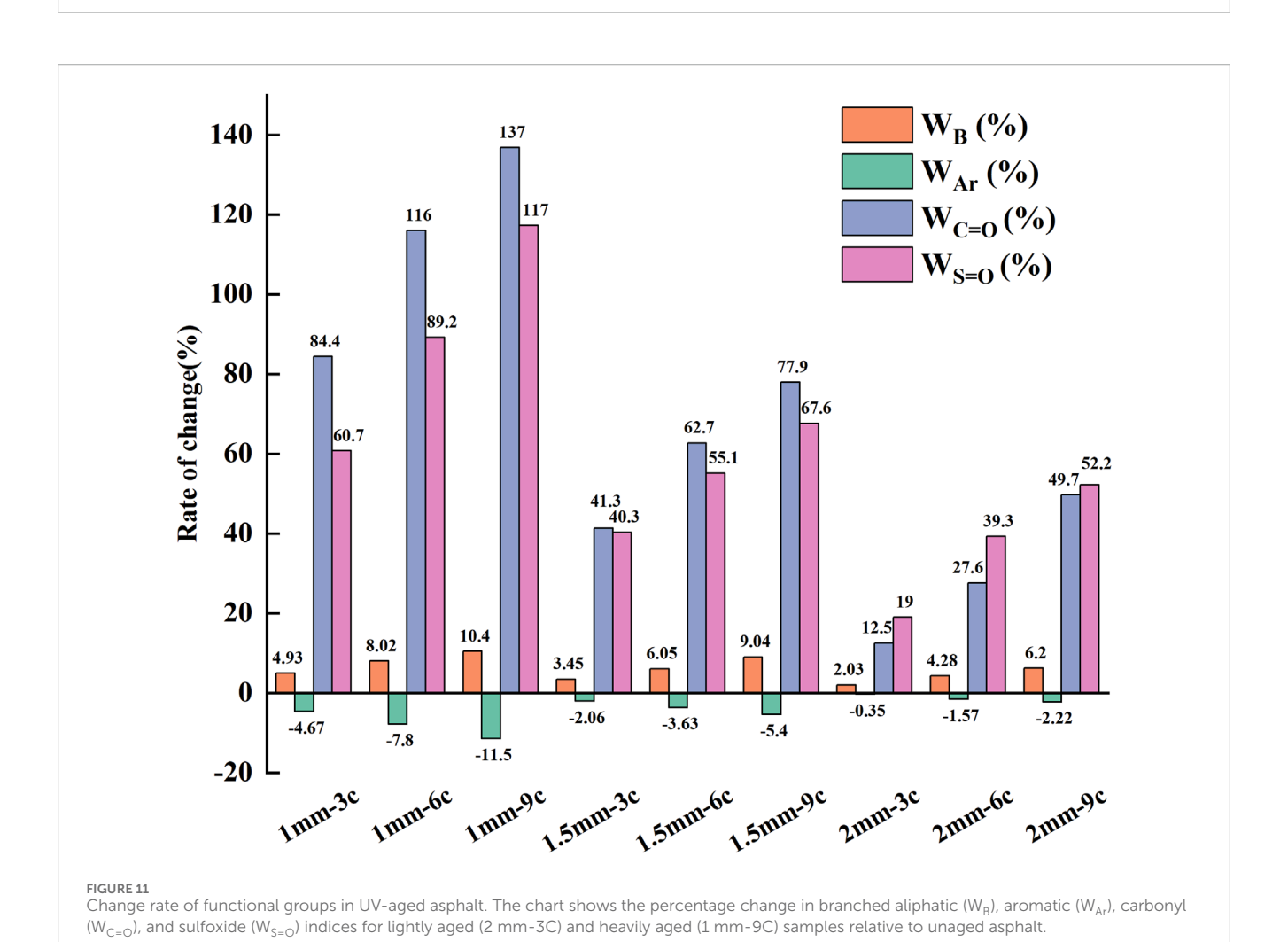
Compared to 90# asphalt, the absorption spectra of UV-aged 1 mm-9C and 2 mm-3C show new overlapping peaks at 1,500 cm<sup>-1</sup> and 3,000 cm<sup>-1</sup>. The peak at 3,000 cm<sup>-1</sup> marks the boundary between saturated and unsaturated hydrocarbons. After UV aging, an overlapping peak appeared in the range of 3,000 cm<sup>-1</sup> to 3,200 cm<sup>-1</sup> due to the formation of unsaturated hydrocarbons. The range of 1,500 cm<sup>-1</sup> to 1800 cm<sup>-1</sup> corresponds to the absorption bands of aromatic compounds, with an overlapping peak at 1,500 cm<sup>-1</sup> associated with the breathing vibrations of the benzene ring framework.

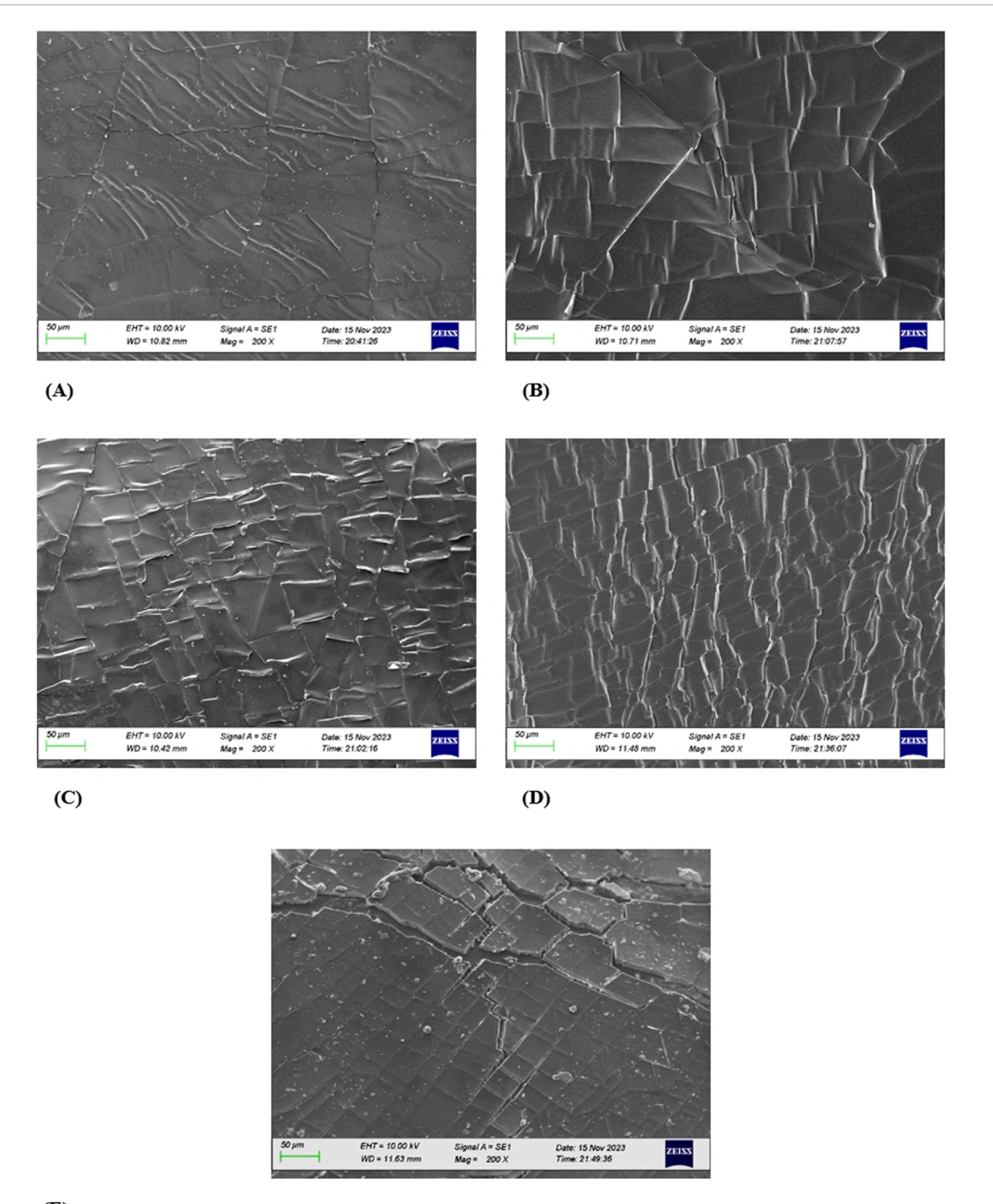
Figure 11 shows that after UV aging, the values for  $W_B$ ,  $W_{C=O}$ , and  $W_{S=O}$  in the aged asphalt are all positive, indicating an increase in the relative content of aliphatic functional groups, carbonyl functional groups, and sulfoxide functional groups. Conversely,  $W_{Ar}$  is negative, representing a reduction in aromatic functional groups. During the UV aging process, molecular chain scission, polycondensation, and oxidation reactions occur, leading to the generation of a substantial amount of carbonyl compounds.

In the UV aging of asphalt, aromatic compounds react to produce aliphatic hydrocarbons, alcohols, and a small amount of aliphatic carboxylic acids. For instance, an absorption peak appears at 970 cm $^{-1}$  in Figure 10, primarily induced by the Norrish II cleavage mechanism, increasing  $\rm I_B$ . A comparison reveals that the values of  $\rm W_B$ ,  $\rm W_{C=O}$ , and  $\rm W_{S=O}$  for the 1 mm-9C sample are the highest, while  $\rm W_{Ar}$  is the lowest. Conversely, in the case of the 2 mm-3C sample, the situation is reversed. As the reaction progresses, aromatic functional groups produce a significant amount of highly



heavily aged (1 mm-9C) samples.





**(E)** 

Shows the crack development process of UV-aged asphalt. The images, taken at 200x magnification, depict the progression of surface damage after (1), (3), (5), (7), and (9) UV aging cycles, from initial wrinkling to large crack formation. (A) 1 mm-1C (slight initial wrinkles on the surface). (B) 1 mm-3C (The wrinkles are deepened and the texture is more obvious). (C) 1 mm-5C (Microcracks begin to appear at the wrinkles). (D) 1 mm-7C (The wrinkles are interconnected to form a network-like crack system). (E) 1 mm-9C (The reticular cracks further developed into large-sized macroscopic cracks with fragmentation phenomenon, indicating that the material has been severely deteriorated).

aromatic hydrocarbons and colloids, while oxidation leads to the scission of side chains in polycyclic aromatic hydrocarbons, resulting in the formation of partially saturated alkanes.

After undergoing oxidation reactions, the concentration of  $I_{S=O}$  increases in sulfur-containing compounds. The generated sulfur phenols and thiols are highly reactive and can promote the formation of a substantial amount of colloids. Through the interactions of sulfur and nitrogen compounds, polyesters and semi-esters generate large molecular colloids, ultimately leading to the formation of asphaltenes.

The value of  $I_{C=O}$  increases with the extent of UV aging, as carbon bonds within the asphalt molecules break. Under UV radiation, these broken bonds react with oxygen to form compounds containing C=C and carbonyl groups. Upon reaching a certain concentration of free radicals as a result of these reactions, chain termination reactions can occur. Consequently, the UV aging process slows down. As the aging asphalt gradually penetrates the deeper layers of asphalt, the concentration at the surface decreases, allowing the UV aging reactions to continue.

FTIR results indicate that photo-oxidation reactions lead to a significant increase in polar oxygen-containing functional groups, primarily carbonyl (C=O) and sulfoxide (S=O) groups. At the molecular level, the formation of these polar groups enhances intermolecular forces, promoting the aggregation of large molecules such as asphaltenes to form more stable and larger molecular clusters.

This microstructural change directly impacts the macroscopic rheological performance. At high temperatures, this stronger molecular network structure inhibits the material's viscous flow, causing it to exhibit a more elastic response. Macroscopically, this is manifested as an increase in the rutting factor and a decrease in the Jnr, thereby enhancing its rutting resistance. However, this hardening effect is detrimental to fatigue performance. The enhanced intermolecular forces restrict the mobility of the asphalt's molecular chains, reducing its ability to relax stress and dissipate energy, making the material stiffer and more brittle overall. Consequently, during the LAS test, the material cannot effectively accommodate deformation, leading to easier micro-crack initiation and propagation, which ultimately manifests as a significant reduction in fatigue life.

# 4.2 Scanning electron microscope analysis (SEM)

Under a constant temperature setting of 60 °C, the surface of UV-aged asphalt still exhibits wrinkling and cracking. As the degree of UV aging increases, wrinkles and cracks gradually develop from the surface inward, leading to a rougher texture and a more pronounced distribution of cracks, as shown in Figure 12.

To reveal the crack formation process in asphalt under UV radiation, aged asphalt samples were re-prepared using a 10 mm diameter silicone mold to cast the asphalt, achieving a film thickness of 1 mm. The cast asphalt samples were removed from the mold and placed on silicone oil paper for UV lamp irradiation, with UV intensity and exposure times corresponding to 1, 3, 5, 7, and 9 cycles.

As shown in Figure 12, SEM was performed at 200x magnification for the asphalt aged for 1, 3, 5, 7, and 9 cycles.

The crack formation process can be divided into five stages corresponding to the aging cycles: (1) Initial wrinkling: After one cycle of UV aging, slight wrinkles and small block-like patterns appear on the surface of the asphalt, with clearly visible lines. At this point, the asphalt still retains some flexibility and stress relaxation capacity, and no actual cracks have formed. (2) Deepening wrinkles: The depth of the surface wrinkles further increases, becoming more pronounced, and the larger patterns gradually refine into slightly smaller lines, yet no cracks appear, and the asphalt still retains some elasticity. (3) Wrinkle deformation: With continued UV lamp exposure, the surface of the asphalt gradually hardens, and the wrinkles begin to develop cracks. Transverse and longitudinal cracks intersect, breaking up the larger patterns into smaller sections, deepening the wrinkles. (4) Formation of web-like cracking: Extensive wrinkles further refine into smaller units divided by transverse and longitudinal cracks, with nearly every small section of asphalt exhibiting raised edges. A network of cracks develops between these sections, with irregular cracking intensifying, indicating severe aging of the asphalt. As the surface cracks, UV light penetrates deeper into the asphalt, accelerating the aging of the underlying layers. (5) Formation of large cracks: After 9 cycles of UV aging, the surface of the asphalt cracks, leading to significant fragmentation, with some areas even crumbling. At this stage, the asphalt has severely aged, becoming hard and brittle.

# 4.3 Atomic force microscopy analysis (AFM)

Figure 13 shows the AFM scan of 90# asphalt and Figure 14 shows the AFM scan of asphalt. The area of the bee structures was calculated by ImageJ image processing. The results of the calculations are shown in Figure 14. The UV aging affects the size of the "bee structures" and their percentage of area in the asphalt. The average area of a single bee structure in UV-aged asphalt exceeds that of 90# asphalt. Figure 15 reveals that UV aging influences both the size of 'bee structures' and their areal proportion in the asphalt. In UV-aged asphalt, the average area of individual bee structures exceeds that found in 90# asphalt. The 1 mm-9C shows a 248% increase in average individual structure area, making its total average area approximately 3.5 times that of 90# asphalt. Even the lightly 2 mm-3C has an average bee structure area that is 22% larger than that of 90# asphalt.

The observed enlargement of the bee structures is entirely consistent with established microstructural aging mechanisms in asphalt. It is widely reported in the literature that the 'bee structure' is a distinct phase domain consisting of a core of highly polar asphaltene micelles surrounded by a less polar maltene phase (Das et al., 2016). During UV aging, photo-oxidation reactions promote the transformation of less polar aromatic components into more polar resins and, ultimately, asphaltenes. This increase in asphaltene concentration, along with the enhanced polarity differences among components, drives molecular aggregation and flocculation (Zhang et al., 2020). Consequently, the asphaltene-rich domains—the bee structures—grow in size. Therefore, our findings provide direct morphological evidence for the phase separation and molecular rearrangement that occurs within asphalt as a result of photo-aging.

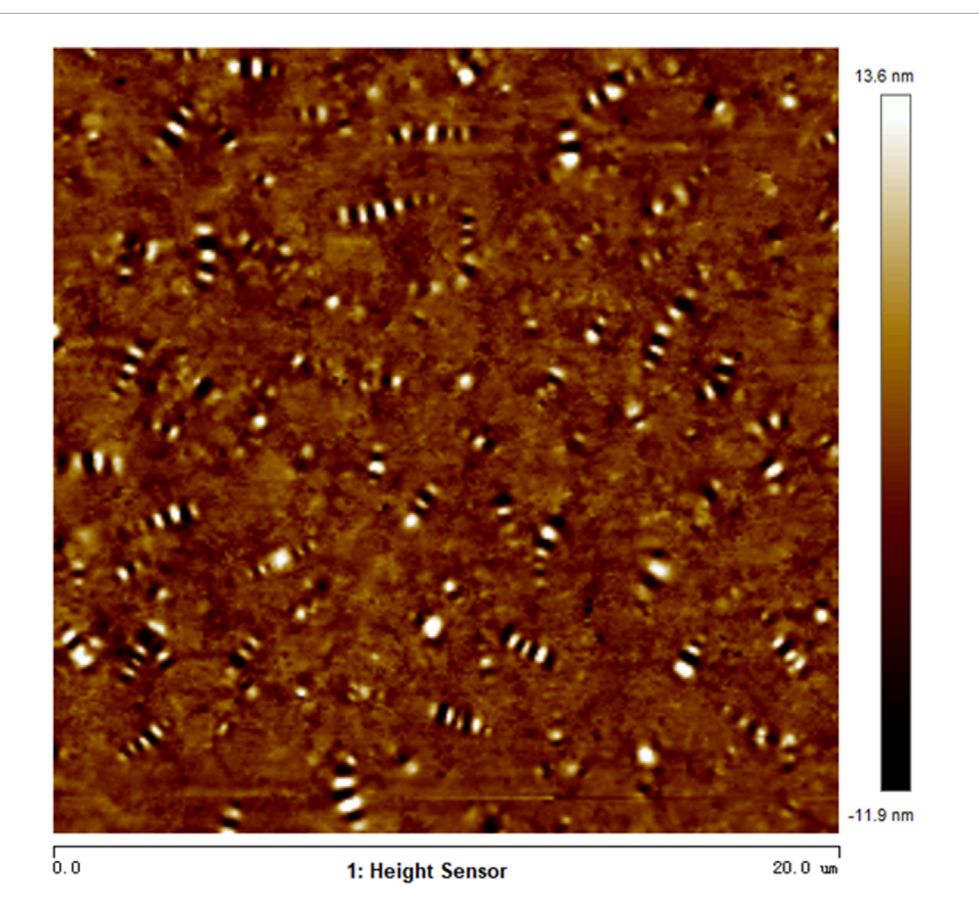


FIGURE 13
AFM scanning image of 90# asphalt. AFM topography of unaged 90# asphalt. The 20  $\mu$ m  $\times$  20  $\mu$ m scan shows the typical 'bee structure' morphology on the surface of the original asphalt sample.

In the selected area, most UV-aged asphalt samples exhibit a smaller areal proportion of bee structures compared to 90# asphalt. Nevertheless, the areal proportion of these structures does not change significantly with variations in film thickness or aging cycles. This observation is attributed to the concurrent increase in the average size of individual 'bee structures' and a decrease in their quantity; these opposing effects result in a total areal proportion that does not show a clear trend with film thickness or aging cycles.

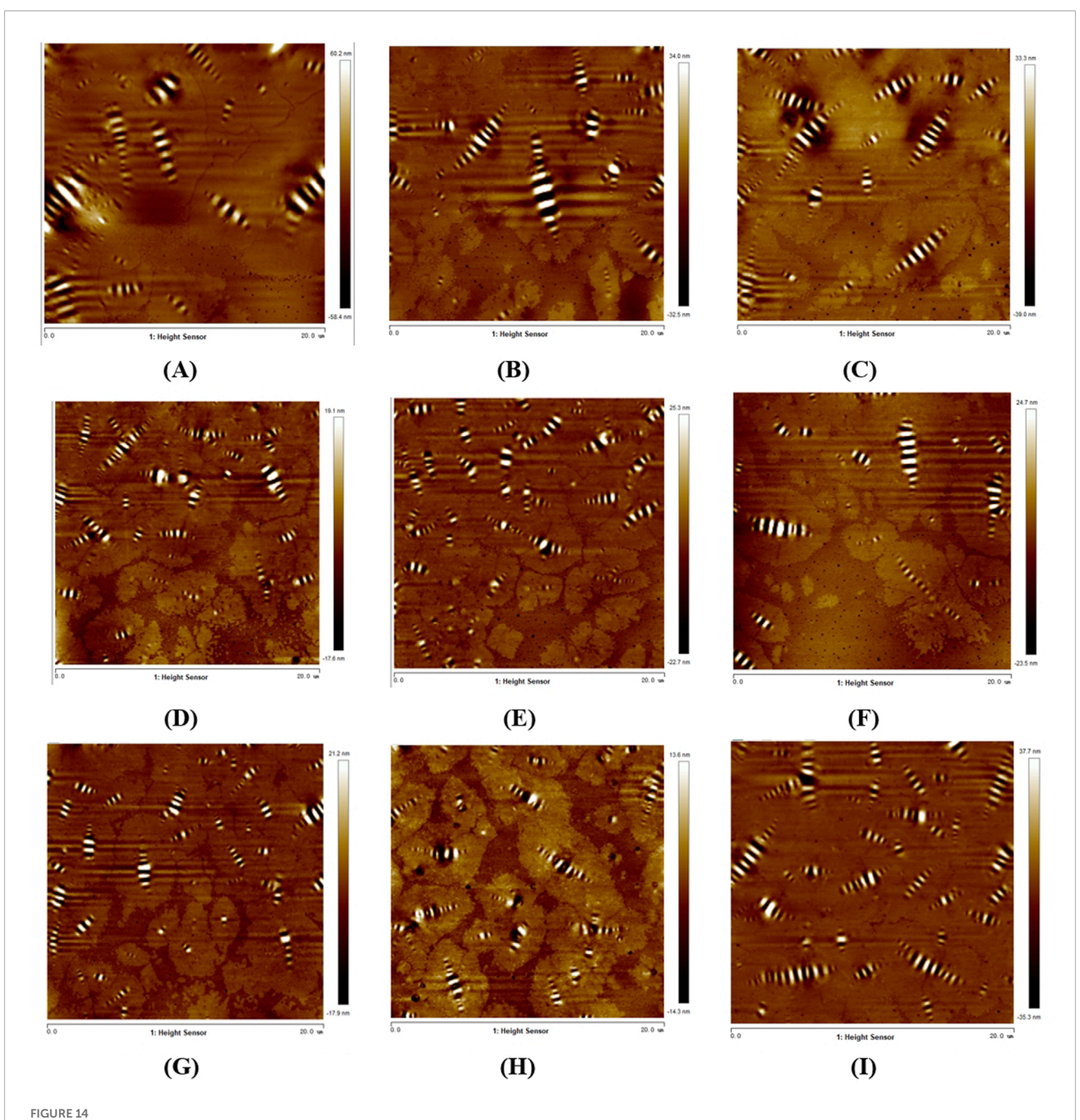
### 5 Conclusion

The core finding of this study is that during laboratory-simulated ultraviolet aging, the thickness of the asphalt film is a more critical influencing factor than the aging cycle. Due to the limited penetration depth of ultraviolet light, the aging effect is mainly concentrated on the material's surface layer. This causes the overall performance degradation of 1 mm thick asphalt samples to far exceed that of 2 mm thick asphalt samples, with more severe increases in their rutting factor and decreases in fatigue life. This finding quantifies the understanding of the film thickness effect from previous research and clarifies that standardizing film thickness is a prerequisite for ensuring the validity of results when evaluating and comparing the UV aging resistance of different asphalts.

This study further reveals the intrinsic connection between the degradation of asphalt's macroscopic properties and the evolution of its microstructure. The macroscopically observed phenomena, such as enhanced high-temperature stability, increased elastic recovery, and decreased fatigue performance, are fundamentally caused by microstructural changes induced by ultraviolet radiation. FTIR analysis confirms the chemical process of oxidative hardening, where oxygen-containing functional groups like carbonyl and sulfoxide significantly increase, while aromatic compounds decrease. Meanwhile, AFM and SEM, respectively, captured, from a morphological perspective, the coalescence and growth of 'bee structures' and the five evolutionary stages of the surface from micro-wrinkling to macro-cracking. This multi-scale evidence collectively constructs a complete damage chain from the breaking of chemical bonds to the final cracking of the material, deepening the understanding of the photo-oxidative failure mechanism of asphalt.

The observed test results must be linked to the actual road surface. In asphalt mixtures, the asphalt binder is wrapped on the surface of the aggregate in the form of a film of  $5-15\,\mu m$ . The crack mechanism observed by SEM directly leads to the cracking and embrittlement of the asphalt binder, which will further lead to pavement diseases such as looseness and cracks.

Based on the above findings, for laboratory standards, any standardized UV aging test protocol must strictly specify and

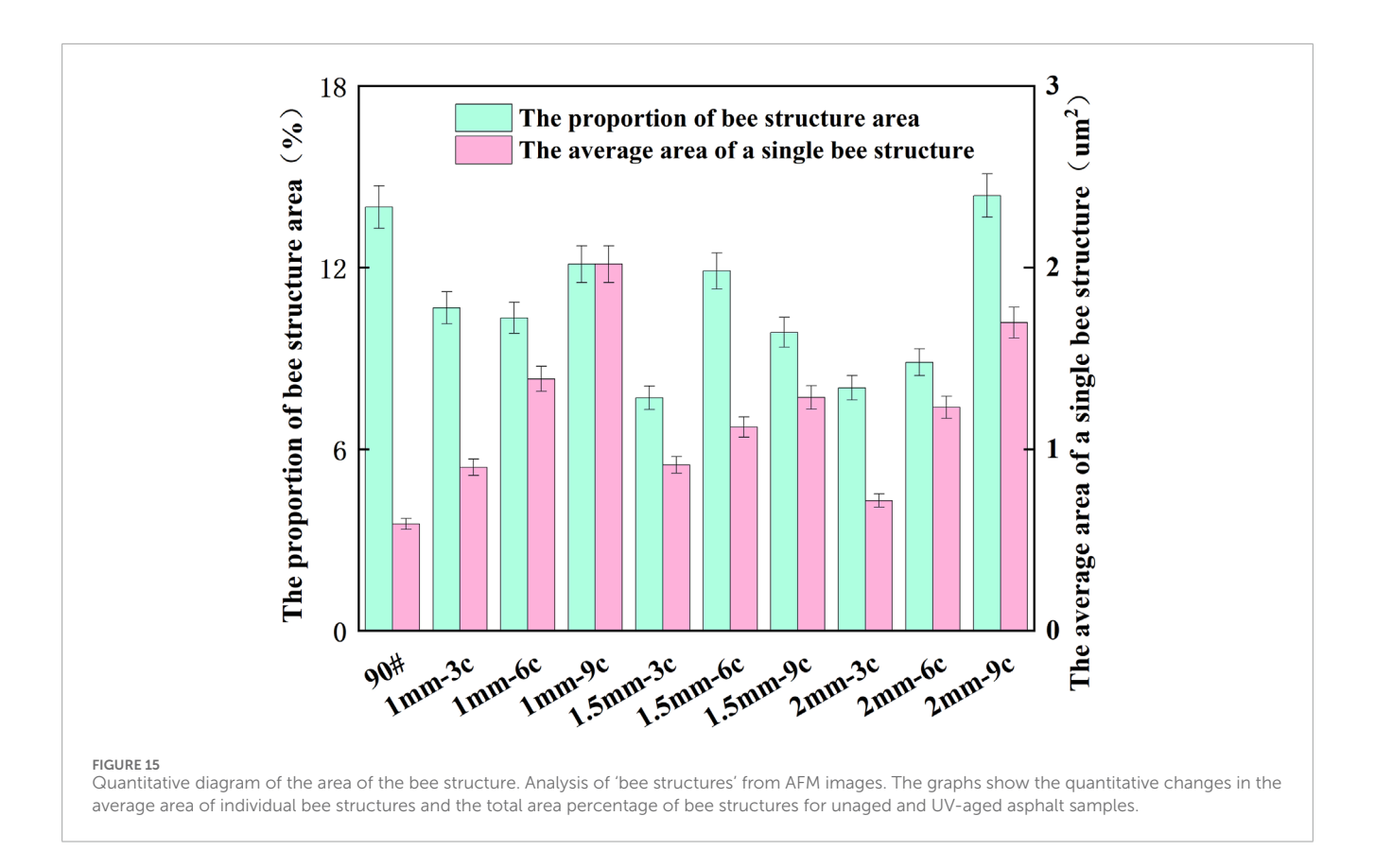


Microscopic morphology of UV-aged asphalt. Representative 20  $\mu$ m  $\times$  20  $\mu$ m AFM scans for asphalt with film thicknesses of (A) 1 mm, (B) 1.5 mm, and (C) 2 mm after 9 aging cycles. (A) AFM results for 1mm-3C. (B) AFM results for 1mm-6C. (C) AFM results for 1mm-9C. (D) AFM results for 1.5mm-3C. (E) AFM results for 1.5mm-6C. (F) AFM results for 1.5mm-9C. (G) AFM results for 2mm-3C. (H) AFM results for 2mm-3C. (I) AFM results for 2mm-9C.

control the sample film thickness to reduce the bias of results. A multi-scale comprehensive evaluation system that combines the macroscopic aging index with the microscopic crack development stage is suggested to achieve more accurate performance evaluation.

The programmable aging model used in this study, although based on actual regional radiation data, represents a simplified

laboratory condition that does not fully replicate the real-world environment. Factors such as humidity, precipitation, cloud cover, and temperature changes can also affect the aging process. Therefore, calibration between real UV exposure and laboratory UV simulations is a necessary step in the future before this work can meaningfully contribute to the development of a final UV aging standard.



# Data availability statement

The raw data supporting the conclusions of this article will be made available by the authors, without undue reservation.

## **Author contributions**

ZL: Data curation, Conceptualization, Writing – original draft, Validation, Writing – review and editing, Formal Analysis, Methodology. XW: Writing – original draft, Visualization, Formal Analysis, Investigation. GH: Software, Formal Analysis, Writing – original draft, Validation, Investigation. YX: Conceptualization, Writing – original draft, Methodology, Formal Analysis. DW: Formal Analysis, Writing – original draft, Software, Methodology.

# **Funding**

The authors declare that financial support was received for the research and/or publication of this article. This work was supported by the Construction Science and Technology Project of the Department of Transportation of Inner Mongolia Autonomous Region (NJ-2020-07), the Research on Nonlinear Fatigue Damage Characteristics of Highway Asphalt Pavement in Cold Regions (2024ZKHX045).

# Acknowledgements

Thank all those who have assisted the author in their work.

#### Conflict of interest

Authors XW, YX, and DW were employed by Ulanqab Transportation Resources Development Group Co., Ltd.

The remaining authors declare that the research was conducted in the absence of any commercial or financial relationships that could be construed as a potential conflict of interest.

#### Generative AI statement

The authors declare that no Generative AI was used in the creation of this manuscript.

Any alternative text (alt text) provided alongside figures in this article has been generated by Frontiers with the support of artificial intelligence and reasonable efforts have been made to ensure accuracy, including review by the authors wherever possible. If you identify any issues, please contact us.

### Publisher's note

All claims expressed in this article are solely those of the authors and do not necessarily represent those of their affiliated

organizations, or those of the publisher, the editors and the reviewers. Any product that may be evaluated in this article, or claim that may be made by its manufacturer, is not guaranteed or endorsed by the publisher.

### References

- Airey, G. D., Grenfell, J. R. A., Apeagyei, A., Subhy, A., and Lo Presti, D. (2016). Time dependent viscoelastic rheological response of pure, modified and synthetic bituminous binders. *Mech. Time-Depend. Mater.* 20, 455–480. doi:10.1007/s11043-016-9295-y
- Capayova, S., Cihlarova, D., and Mondschein, P. (2022). Effect of winter road maintenance on the asphalt road surface-experience in Slovakia and the Czech Republic. *Materials* 15, 5618. doi:10.3390/ma15165618
- Carmona, J. A., Ramirez, P., Calero, N., and Munoz, J. (2023). Effect of the welan gum concentration on the rheological and structural behaviour of biocomposite hydrogels with sepiolite as filler. *Polymers* 15, 33. doi:10.3390/polym15010033
- Celauro, C., Teresi, R., and Dintcheva, N. T. (2022). Effect of short-term and UV irradiation aging on the behaviour of SBS-modified bitumen. *Sustainability* 14, 6915. doi:10.3390/su14116915
- Chen, Z., Zhang, H., and Duan, H. (2020). Investigation of ultraviolet radiation aging gradient in asphalt binder. *Constr. Build. Mater.* 246, 118501. doi:10.1016/j.conbuildmat.2020.118501
- Cong, P., Wang, J., Li, K., and Chen, S. (2012). Physical and rheological properties of asphalt binders containing various antiaging agents. *Fuel* 97, 678–684. doi:10.1016/j.fuel.2012.02.028
- Das, P. K., Baaj, H., Tighe, S., and Kringos, N. (2016). Atomic force microscopy to investigate asphalt binders: a state-of-the-art review. *Road Mater. Pavement Des.* 17, 693–718. doi:10.1080/14680629.2015.1114012
- Durrieu, F., Farcas, F., and Mouillet, V. (2007). The influence of UV aging of a styrene/butadiene/styrene modified bitumen: Comparison between laboratory and on site aging. *Fuel* 86, 1446–1451. doi:10.1016/j.fuel.2006.11.024
- Feng, Z., Bian, H., Li, X., and Yu, J. (2016). FTIR analysis of UV aging on bitumen and its fractions. *Mater. Struct.* 49, 1381–1389. doi:10.1617/s11527-015-0583-9
- Godenzoni, C., Graziani, A., and Perraton, D. (2017). Complex modulus characterisation of cold-recycled mixtures with foamed bitumen and different contents of reclaimed asphalt. *Road. Mater. Pavement Des.* 18, 130–150. doi:10.1080/14680629.2016.1142467
- Guo, M., Yin, X., Liang, M., and Du, X. (2023). Study on effect of thermal, oxidative and ultraviolet coupled aging on rheological properties of asphalt binder and their contribution rates. *Int. J. Pavement Eng.* 24, 2239426. doi:10.1080/10298436.2023.2239426
- He, Y., Hu, Q., Zhao, X., Zhang, J., Lyu, L., Li, Y., et al. (2025a). Impacts of ultraviolet irradiation on asphalt binder: a comprehensive review. *Int. J. Pavement Eng.* 26, 2472839. doi:10.1080/10298436.2025.2472839
- He, Z., Geng, J., Zhao, W., Liu, J., Qi, C., Qi, R., et al. (2025b). Road performance and chemical evolution of aged asphalt subjected to intense ultraviolet radiation and large temperature fluctuations. *Fuel* 394, 135104. doi:10.1016/j.fuel.2025.135104
- Hu, J., Wu, S., Liu, Q., Hernandez, M. I. G., Zeng, W., and Xie, W. (2017). Study of antiultraviolet asphalt modifiers and their antiageing effects. *Adv. Mater. Sci. Eng.* 2017, 1–9. doi:10.1155/2017/9595239
- Hu, J., Wu, S., Liu, Q., García Hernández, M. I., Zeng, W., Nie, S., et al. (2018). The effect of ultraviolet radiation on bitumen aging depth. *Materials* 11, 747. doi:10.3390/ma11050747
- Li, Y., Wu, S., Liu, Q., Dai, Y., Li, C., Li, H., et al. (2019a). Aging degradation of asphalt binder by narrow-band UV radiations with a range of dominant wavelengths. *Constr. Build. Mater.* 220, 637–650. doi:10.1016/j.conbuildmat.2019.06.035
- Li, Y., Wu, S., Liu, Q., Xie, J., Li, H., Dai, Y., et al. (2019b). Aging effects of ultraviolet lights with same dominant wavelength and different wavelength ranges on a hydrocarbon-based polymer (asphalt). *Polym. Test.* 75, 64–75. doi:10.1016/j.polymertesting.2019.01.025
- Li, W., Hao, P., Liu, G., Li, Z., Le, C., Wang, C., et al. (2025). Research on the microscopic aging characteristics of asphalt binder based on atomic force microscopy. *Polymers* 17, 1000. doi:10.3390/polym17081000

Maraveas, C., Kotzabasaki, M. I., Bayer, I. S., and Bartzanas, T. (2023). Sustainable greenhouse covering materials with Nano- and micro-particle additives for enhanced radiometric and thermal properties and performance. *AgriEngineering* 5, 1347–1377. doi:10.3390/agriengineering5030085

Maraveas, C., Kyrtopoulos, I. V., Arvanitis, K. G., and Bartzanas, T. (2024). The aging of polymers under electromagnetic radiation. *Polymers* 16, 689. doi:10.3390/polym16050689

Mouillet, V., Farcas, F., Chailleux, E., and Sauger, L. (2014). Evolution of bituminous mix behaviour submitted to UV rays in laboratory compared to field exposure. *Mater. Struct.* 47, 1287–1299. doi:10.1617/s11527-014-0258-y

Petersen, J. C., Robertson, R. E., Branthaver, J. F., Harnsberger, P. M., Duvall, J. J., Kim, S. S., et al. (1994). *Binder characterization and evaluation. Volume 1*. Washington, DC: The National Academies of Sciences, Engineering, and Medicine. Available online at: https://trid.trb.org/View/405682 (Accessed October 14, 2025).

Polo-Mendoza, R., Martinez-Arguelles, G., Walubita, L. F., Moreno-Navarro, F., Giustozzi, F., Fuentes, L., et al. (2022). Ultraviolet ageing of bituminous materials: a comprehensive literature review from 2011 to 2022. *Constr. Build. Mater.* 350, 128889. doi:10.1016/j.conbuildmat.2022.128889

- Ren, D., Xiong, W., Fan, S., Luo, Y., Jin, X., Lai, F., et al. (2025). Surface functionalization of MXene with gallic acid for enhanced UV aging resistance in SBS-modified asphalt: a study of interface interaction and molecular dynamics. *Colloids Surfaces A Physicochem. Eng. Aspects* 711, 136316. doi:10.1016/j.colsurfa.2025.136316
- Siddiqui, M. N., and Ali, M. F. (1999). Studies on the aging behavior of the Arabian asphalts. Fuel 78, 1005–1015. doi:10.1016/S0016-2361(99)00018-6
- Sun, X., Xu, Q., Fang, G., Zhu, Y., Yuan, Z., Chen, Q., et al. (2022). Effect investigation of ultraviolet ageing on the rheological properties, micro-structure, and chemical composition of asphalt binder modified by modifying polymer. *Adv. Mater. Sci. Eng.* 2022, 1–19. doi:10.1155/2022/7190428
- Wang, C., Tian, X. G., Wang, Y., and Li, G. (2024a). Asphalt aging and its antiaging mechanism based on quantum chemistry. *Case Stud. Constr. Mater.* 20, e02802. doi:10.1016/j.cscm.2023.e02802
- Wang, Z., Ding, H., Ma, X., Yang, W., and Ma, X. (2024b). Predicting dynamic properties and fatigue performance of aged and regenerated asphalt using time-temperature-aging and time-temperature-regenerator superposition principles. *Coatings* 14, 1486. doi:10.3390/coatings14121486
- Xiao, M. M., and Fan, L. (2022). Ultraviolet aging mechanism of asphalt molecular based on microscopic simulation. *Constr. Build. Mater.* 319, 126157. doi:10.1016/j.conbuildmat.2021.126157
- Zadshir, M., Hosseinnezhad, S., Ortega, R., Chen, F., Hochstein, D., Xie, J., et al. (2018). Application of a biomodifier as fog sealants to delay ultraviolet aging of bituminous materials. *J. Mater. Civ. Eng.* 30, 04018310. doi:10.1061/(ASCE)MT.1943-5533.0002483
- Zeng, W., Wu, S., Pang, L., Chen, H., Hu, J., Sun, Y., et al. (2018). Research on ultra violet (UV) aging depth of asphalts. *Constr. Build. Mater.* 160, 620–627. doi:10.1016/j.conbuildmat.2017.11.047
- Zhang, J., Airey, G. D., Grenfell, J., and Yao, Z. (2017). Laboratory evaluation of rediset modified bitumen based on rheology and adhesion properties. *Constr. Build. Mater.* 152, 683–692. doi:10.1016/j.conbuildmat.2017.07.037
- Zhang, H., Chen, Z., Xu, G., and Shi, C. (2018). Evaluation of aging behaviors of asphalt binders through different rheological indices. *Fuel* 221, 78–88. doi:10.1016/j.fuel.2018.02.087
- Zhang, H., Wang, Y., Yu, T., and Liu, Z. (2020). Microstructural characteristics of differently aged asphalt samples based on atomic force microscopy (AFM). *Constr. Build. Mater.* 255, 119388. doi:10.1016/j.conbuildmat.2020.119388
- Zhou, X., Ge, D., Lv, S., Wang, X., Li, Y., and Ju, Z. (2024). Influence of variable intensity ultraviolet on the performance of SBS modified asphalt. *Case Stud. Constr. Mater.* 21, e03854. doi:10.1016/j.cscm.2024.e03854